

The magnetorotational instability in debris-disc gas

Quentin Kral^{1*} & Henrik Latter²

¹*Institute of Astronomy, University of Cambridge, Madingley Road, Cambridge CB3 0HA, UK*

²*DAMTP, University of Cambridge, CMS, Wilberforce Road, Cambridge CB3 0WA, UK*

Accepted 1928 December 15. Received 1928 December 14; in original form 1928 October 11

ABSTRACT

Debris discs are commonly swathed in gas which can be observed in UV, in fine structure lines in FIR, and in resolved maps of CO emission. Carbon and oxygen are overabundant in such gas, but it is severely depleted in hydrogen. As a consequence, its ionisation fraction is remarkably high, suggesting magnetohydrodynamic (MHD) processes may be important. In particular, the gas may be subject to the magnetorotational instability (MRI), and indeed recent modelling of β Pictoris requires an anomalous viscosity to explain the gas’s observed radial structure. In this paper we explore the possibility that the MRI is active in debris-disc gas and responsible for the observed mass transport. We find that non-ideal MHD and dust-gas interactions play a subdominant role, and that linear instability is viable at certain radii. However, owing to low gas densities, the outer parts of the disc could be stabilised by a weak ambient magnetic field, though it is difficult to constrain such a field. Even if the MRI is stabilised by too strong a field, a magnetocentrifugal wind may be launched in its place and this could lead to equivalent (non-turbulent) transport. Numerical simulations of the vertically stratified MRI in conditions appropriate to the debris disc gas should be able to determine the nature of the characteristic behaviour at different radii, and decide on the importance of the MRI (and MHD more generally) on the evolution of these discs.

Key words: instabilities — magnetic fields — MHD — turbulence — interplanetary medium — circumstellar matter

1 INTRODUCTION

Observations of gas in debris discs are becoming increasingly common thanks to the analysis of UV absorption lines (for edge-on discs), detections of C II and O I by Herschel, and highly resolved sub-mm images of CO and the continuum provided by ALMA (e.g. Dent et al. 2014). One of the more important discoveries is that gas in these old systems is not a remnant of their preceding protoplanetary discs, but is continually replenished by the disc’s solid bodies, either by photodesorption (Grigorieva et al. 2007) or grain-grain collisions (Czechowski & Mann 2007).

Amongst debris discs with gas, β Pic is the best constrained. Molecules such as CO (Dent et al. 2014), atoms such as C, O, S, and a variety of metals have been detected in β Pictoris’ gas disc (Roberge et al. 2006). Hydrogen, on the other hand, is thought to be highly depleted (Freudling et al. 1995; Lecavelier des Etangs et al. 2001), and in fact the gas mostly composed of carbon (e.g. Roberge et al. 2014; Cataldi et al. 2014). Partly as a result, the ionisation fraction is exceptionally high: in β Pictoris, it may be close to

0.5 (Cataldi et al. 2014), significantly greater than a protoplanetary disc, though gas densities in debris discs are much less.

Recently, Kral et al. (2016) developed a new model to study the evolution of gas in debris discs. They propose that (a) CO is created within the debris belt (by grain collisions or photodesorption), (b) quickly photodissociated into carbon and oxygen, and then (c) that the two atomic elements spread radially, due to an anomalous viscosity that may be parameterised with the α prescription (Shakura & Sunyaev 1973). The resulting time and radius dependent ionisation fractions, temperature, and number densities of carbon and oxygen are computed using the PDR-like algorithm, Cloudy (Ferland et al. 2013), which is coupled to a 1D dynamical α model for the disc structure. In order to reproduce the gas observations in β Pic, Kral et al. (2016) require the diffusion of gas to be very effective. In other words, there must be significant turbulent activity in order to transfer enough angular momentum. In fact, they predict that $\alpha > 0.1$ in the gas disc. What could be the cause of such a high level of turbulence? Given the typical ionisation fractions, could this transport be the result of the magnetorotational instability

* E-mail: qkral@ast.cam.ac.uk

(MRI, Balbus & Hawley 1998)? It is this question that our paper is concerned with.

Certainly, the highly ionised discs associated with close binaries yield α values ranging from 0.1 to 0.4 in their high states (King et al. 2007), while the accretion discs orbiting Be stars sometimes exhibit even higher values (Carciofi et al. 2012). As the MRI is thought to be responsible for the transport in these systems, so too could it drive gas diffusion in debris discs. Numerical simulations of the MRI also report α values that can reach up to 0.1 (e.g. Sano et al. 2004; Simon et al. 2009; Salvesen et al. 2016). However, the physical conditions in debris-disc gas is potentially different to these classical applications. Of greatest concern is the gas's low density, which make it vulnerable to ambipolar diffusion and the stabilising role of magnetic tension.

In this paper, we check the linear stability of the gaseous envelope of a debris disc to the MRI, focussing on the system that is best characterised: β Pictoris. We use the model presented in Kral et al. (2016) to determine the parameters of its gas disc and then determine its linear stability, following the formalism of Kunz & Balbus (2004, hereafter KB04). We find that, on the whole, non-ideal MHD effects are not crucial, nor is the dust-gas coupling. However, relatively weak fields can stabilise the MRI; at 100 AU, fields greater than a μG are sufficient to deactivate the fastest growing modes (channel flows), though much slower radial-modes can still function, presumably leading to only weak transport. It is possible that at these larger radii a magneto-centrifugal wind supplants the MRI and provide the effective α that observations and modelling demand (Ogilvie 2012; Bai & Stone 2013b; Lesur et al. 2013). We do not examine in detail this and alternative nonlinear outcomes, but future numerical work in vertically stratified boxes tailored to debris disc conditions will be able to determine how the gas radially spreads.

In Section 2, we present the state-of-the-art of gas modelling in debris discs and give some details of the physical regime in which β Pictoris lies. In Section 3 we present the linear theory of the ambipolar MRI and test it on β Pic. Finally, we discuss these results, previous simulation results that are relevant, and point to future work.

2 DEBRIS DISC PROPERTIES

2.1 Debris disc gas

The gas that cocoons debris discs appears depleted in hydrogen but abundant in carbon and oxygen (Zagorovsky et al. 2010; Cataldi et al. 2014). These discs are observed around young main sequence stars where the main ionising fluxes come from the interstellar radiation field (IRF) and the star itself. It is worth pointing out that the main source of ionisation in protoplanetary discs (X-rays produced by stellar coronal activity) is absent at this later evolutionary stage. C I is ionised easily by the IRF (and the stellar radiation field) because its ionisation potential (IP) is 11.26eV, whilst hydrogen and oxygen IPs are 13.6eV, just above the limit set by the Lyman break. One can then regard these discs as mainly composed of C II (ionisation fraction ~ 0.5), C I and O I. Some other metals are observed but in smaller quantities. If it were not for Coulomb collisions with C II,

these metals would leave the system on a few dynamical timescale due to radiation pressure (Fernández et al. 2006; Olofsson et al. 2001). We neglect, however, these relatively scarce metals.

Kral et al. (2016) propose that the gas in debris discs is created within the main belt by either photodesorption or grain-grain collisions. CO is released from the grains and photodissociates quickly into carbon and oxygen. Oxygen remains neutral but carbon becomes ionised. The atomic gas then evolves viscously, due to turbulence parametrised by an α viscosity. As the viscosity depends on temperature, Kral et al. (2016) use a PDR-like code (called ‘Cloudy’) to follow the thermal evolution of the gas at the same time as its dynamics. The temperature is fixed by a competition between the carbon photoionisation heating and the cooling by the C II fine structure line. The free parameters in the model are α , the mass input rate of CO, the location of the debris belt and the amount of UV flux impinging on the gas disc. The CO input rate and location of the debris belt are determined by ALMA observations of β Pic. Once these are fixed, Kral et al. (2016) find that all other observations are reconciled if $\alpha \gtrsim 0.1$. Thus the anomalous transport required is very efficient.

In Fig. 1 we show the best-fit model of the β Pic gas disc in Kral et al. (2016) to give a sense of the physical regime it lies in and which we explore in this paper. The number densities for carbon and oxygen are lower than 10^4 cm^{-3} . The oxygen density equals the sum of the C I and C II densities because these atomic elements arise from the breakup of CO. Because of the depletion of hydrogen, the dynamics of the system and its thermal evolution is controlled by the carbon content. One can see that the C II density profile flattens in the inner region. This is a consequence of the accretion disc structure. The carbon density reaches higher values in the inner region and so the medium becomes optically thick to FUV; as a result, carbon ionisation is impeded (see Fig. 1 right). The electron density is superimposed on the C II line in Fig. 1 (left) as electrons are produced through C I photoionisation. Finally, Kral et al. (2016) showed that the dust does not have any thermal effect on the gas state because the photoelectric effect is not sufficiently strong.

For comparison with a typical protoplanetary disc we employ the Minimum Mass Solar Nebula (MMSN) (Hayashi 1981). At 10AU and 100AU, β Pic surface densities are ~ 8 and $4 \times 10^{-7} \text{ g cm}^{-2}$ whilst the MMSN gives ~ 50 and 1.7 g cm^{-2} . Thus, the debris disc gas possesses a surface density 10^7 times lower than typical protoplanetary discs. However, the ionisation fraction is significantly higher, $\gtrsim 0.1$. In contrast, a protoplanetary disc at 10 AU yields fractions between 10^{-10} (at the midplane) to 10^{-5} in the disc corona (Lesur et al. 2014). Finally, the ionisation timescale in β Pic is found to be on the order of a few years, which is markedly shorter than the local orbital period everywhere for the radial range considered in Fig. 2.

The temperature varies between ~ 110 and 20K for β Pic, but is not a simple power law as shown by Fig. 2 (left). Three regimes can be observed as explained in Kral et al. (2016). In most of the disc, the temperature drops as $R^{-0.8}$ (before flattening out) due to the increasing ionisation fraction of carbon, which provides more C II to cool the system. The absolute value of the temperature and the profile is similar to what is expected in protoplanetary discs (e.g. Bell et

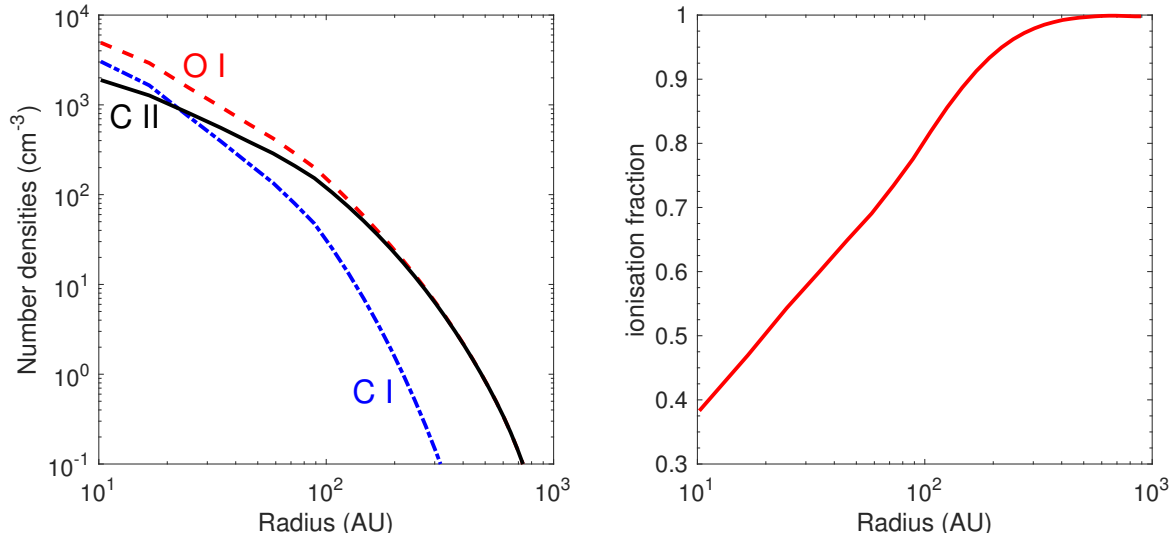


Figure 1. β Pic best-fit model from Kral et al. (2016). *Left:* Densities of C I (dashed-dotted blue), C II (solid black) and O I (dashed red). The electron density is the same as the C II density. *Right:* Carbon ionisation fraction as a function of R .

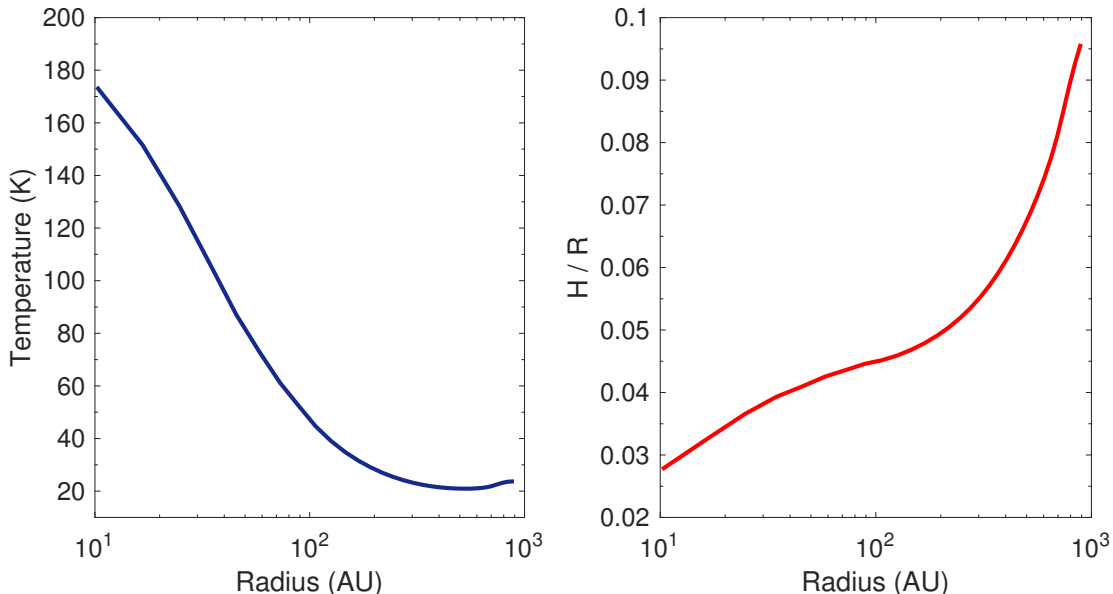


Figure 2. β Pic best-fit model from Kral et al. (2016). *Left:* Temperature as a function of R . *Right:* H/R over R as a function of R .

al. 1997). The derived H/R is shown on Fig. 2 (right) and varies between ~ 0.03 at 10 AU and 0.1 at 1000 AU.

2.2 Non-ideal MHD

Owing to the low number densities, and the consequently weaker collisional coupling, one may expect non-ideal MHD effects to raise their heads. The importance of these effects may be quantified by the Elsasser numbers for Ohmic diffusion, the Hall effect, and ambipolar diffusion. The first two

are given by

$$E_O = \left(\frac{4\pi e^2}{c^2 m_e \Omega} \right) \frac{x_e}{\langle \sigma v \rangle_{ne} + \langle \sigma v \rangle_{ie}} v_A^2, \quad E_H = \frac{B e x_e}{m_n \Omega c} \quad (1)$$

respectively. Here Ω is the orbital period, c is the speed of light, x_e is the electron fraction, m_e and m_n are the masses of electrons and neutrals, e is charge, B is the imposed magnetic field, and $v_A = B/\sqrt{4\pi\rho}$ is the Alfvén speed (with ρ mass density of the fluid). Finally, $\langle \sigma v \rangle_{ne} \sim 8.28 \times 10^{-9} (T/100K)^{0.5} \text{ cm}^3 \text{ s}^{-1}$ and $\langle \sigma v \rangle_{ie} \sim 0.37 \ln \lambda / 17 (T/100K)^{-1.5} \text{ cm}^3 \text{ s}^{-1}$, where $\ln \lambda$ is the Coulomb logarithm. Estimates for the two Elsasser num-

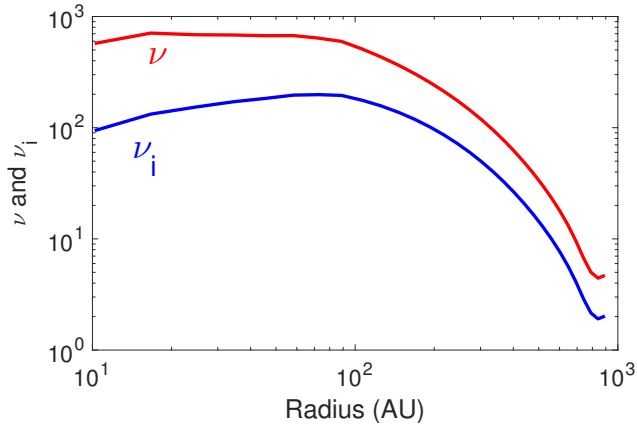


Figure 3. β Pic best-fit model from Kral et al. (2016). ν (red) and ν_i (blue) as a function of R (see Eq. 4).

bers are captured by the following scalings

$$E_{\text{O}} \sim 1.3 \times 10^6 \left(\frac{T}{100 \text{ K}} \right)^{5/2} \left(\frac{R}{10 \text{ AU}} \right)^{3/2} \beta^{-1} x_e \left(\frac{\ln \lambda}{17} \right)^{-1}, \quad (2)$$

$$E_{\text{H}} \sim 4.8 \times 10^5 \left(\frac{T}{100 \text{ K}} \right)^{1/2} \left(\frac{R}{10 \text{ AU}} \right)^{3/2} \left(\frac{n}{100 \text{ cm}^{-3}} \right)^{1/2} \beta^{-1/2} x_e, \quad (3)$$

where $\beta = 2c_s^2/v_A^2$ is the plasma beta. Clearly in the case of β Pic, these quantities are extremely large, and Ohmic and Hall effects can safely be ignored.

The Elsasser number for Ambipolar diffusion, sometimes just called the ambipolar parameter, is the normalised collision rate between ions and neutral. We define it via

$$\nu_i = \frac{\gamma \rho_i}{\Omega}, \quad (4)$$

where ρ_i is the mass density of the ions, and γ is the drag coefficient. It may be calculated via $\gamma = \langle \sigma v \rangle_i / (m_n + m_i)$, with $\langle \sigma v \rangle_i = 9.57 \times 10^{-10} \text{ cm}^3 \text{ s}^{-1}$ the ion-neutral (C^+/O) collision rate (Draine 2011). An equivalent parameter can be computed for the total fluid which we denote by ν . Both ν_i and ν are plotted in Figure 3. At most radii both are ~ 100 , and thus neutrals and ions are relatively well coupled. Consequently, ambipolar diffusion is not dominant though, as we shall see in the next section, its effects are not always negligible.

2.3 Dust-gas interactions

Of course, debris discs are composed of a dusty component that could interfere with the gas dynamics, and vice versa. In this subsection we explore the coupling between gas and dust to see whether it could affect the onset of MRI.

The dust number density n_d in β Pic varies between 10^{-11} to 10^{-10} cm^{-3} , from 10 to 200AU (Heap et al. 2000; Zagorovsky et al. 2010). The mass density is less or comparable to that of the gas in the system. As a comparison, the mass density of the dust in protoplanetary discs is usually taken to be only 1% of the gas. Running the model presented

in Kral et al. (2016), we find that in general dust grains in debris discs are charged positively with a mean charge of $\sim 10q$. We also find that the vast majority of electrons in the gas come from photoionisation of carbon rather than the dust’s photoelectric effect.

As regards the gas’s effect on the dust dynamics, Kral et al. (2016) show that gas drag is only important for the smallest grains, which are scarce in any case because they fall below the blow-out-size (e.g. Kral et al. 2013). For the most numerous grain sizes the Stokes number of the dust fluid is > 10 .

Next we assess the dust’s effect on gas dynamics, focusing on β Pic. The neutral-atom/dust collision frequency p can be estimated from

$$\frac{p}{\Omega} = 2 \times 10^{-4} \left(\frac{d}{5 \mu\text{m}} \right)^2 \left(\frac{n_d}{10^{-10} \text{ cm}^{-3}} \right) \left(\frac{T}{50 \text{ K}} \right)^{0.5} \left(\frac{R}{10 \text{ AU}} \right)^{1.5}, \quad (5)$$

where d is the grain size. In debris discs, the collisional cross-section is dominated by the smallest dust grains close to the blow-out size; the parameters in Eq. 5 account for that. Even in the worst case scenario for grains that are at hundreds of AU, p/Ω is always smaller than 10^{-2} . This estimate indicates there is only weak coupling between the neutral atoms and dust grains. The two fluids are mostly free to pursue their own dynamics separately.

However, grains are strongly charged which can increase the collisional cross-section with ions and electrons. We used Draine & Sutin (1987) to quantify the increase in collisional cross section for charged grains. The ϵ variable in Draine & Sutin (1987) is defined by $\epsilon = E d/e^2$, where E is the kinetic energy of an ion of charge $-e$. For charged grains in β Pic it may be estimated by

$$\epsilon = 4 \times 10^4 \left(\frac{d}{5 \mu\text{m}} \right) \left(\frac{R}{10 \text{ AU}} \right)^{-1}, \quad (6)$$

which is relatively high because of the size of the grains and their significant charge. Using this value for ϵ and the average grain charge, Fig. 1 in Draine & Sutin (1987) indicates that the collisional cross-section is not greatly enhanced. Thus the Eq. 5 is a good estimate for all constituents of the gas fluid.

As a consequence, dust drag is neglected in the following section, though is easy to include and may be relevant for debris discs in which the dust density is higher. The drag should only influence the MRI when the collision frequency is $\sim \Omega$. In this case, the MRI growth rate is decreased, though the instability criterion is not altered directly, as shown by Guilet et al. (2015) in the context of protoneutron stars.

3 THE MRI IN DEBRIS DISCS

In this section we briefly present a MRI stability analysis tailored to the partially ionised plasma swathing debris discs. The formalism is lifted from KB04 who include the effects of ion-neutral drift (ambipolar diffusion) in a single fluid treatment.

As is clear from Figure 3, the coupling timescales of both ions and neutrals is much less than the orbital timescale throughout most of the disc, both ν and ν_i are ~ 100 on

radii less than ~ 100 AU. Thus, the collisional coupling between the ions and neutrals remains sufficiently high for a single-fluid model to be applicable. For reference, the outer regions of a protoplanetary disc possess $\nu \sim 10^9$ and $\nu_i \sim 10$ (e.g. Bai 2011; Simon et al. 2015). Moreover, the electron recombination time is short compared to the local orbital period. Ambipolar diffusion plays a relatively minor role, but we retain its effects in the model. Both the Hall effect and Ohmic diffusion are omitted. Their respective Elsasser numbers exceed 10^5 and thus we deem them to be very much subdominant.

It should be stressed that gas in other debris discs may be more dilute and less well ionised, in which case the two-fluid model of Blaes & Balbus (1994) may be more appropriate. This will certainly be the case if equilibrium ionisation chemistry is included: as those authors show, an increasing azimuthal field markedly reduces the MRI growth rates, and indeed complete stabilisation is possible. Note that β Pic is too dense for this effect to be important.

3.1 Governing equations

We assume the MRI instigates relatively slow motions and excites relatively short scales. We thus adopt the equations of incompressible non-ideal MHD and a local model of the disc (the shearing box; Goldreich & Lynden-Bell 1965). The latter is a corotating Cartesian representation of a small ‘block’ of disc fluid at a given radius R_0 orbiting at a rate Ω . Its radial and azimuthal coordinates are denoted by x and y , respectively.

The equations controlling the evolution of the neutral fluid are

$$\partial_t \mathbf{v} + \mathbf{v} \cdot \nabla \mathbf{v} = -\frac{1}{\rho} \nabla p - \nabla \Phi_t - 2\Omega \mathbf{e}_z \times \mathbf{v} + \frac{(\nabla \times \mathbf{B}) \times \mathbf{B}}{4\pi\rho}, \quad (7)$$

$$\partial_t \mathbf{B} + \mathbf{v} \cdot \nabla \mathbf{B} = \mathbf{B} \cdot \nabla \mathbf{v} + \nabla \times \left[\frac{(\mathbf{J} \times \mathbf{B}) \times \mathbf{B}}{c\gamma\rho_i\rho} \right], \quad (8)$$

where \mathbf{v} , ρ , and p are the neutral fluid’s velocity, density, pressure, while \mathbf{B} is the magnetic field. The tidal potential is given by $\Phi_t = -(3/2)\Omega^2 x^2$, and the current density by $\mathbf{J} = (c/4\pi)\nabla \times \mathbf{B}$. The ion density is denoted by ρ_i and c is the speed of light. These equations must be solved alongside the solenoidal restrictions, $\nabla \cdot \mathbf{v} = \nabla \cdot \mathbf{B} = 0$.

3.2 Dispersion relation

We assume for simplicity a homogeneous equilibrium of simple Keplerian rotation so that ρ is a constant, and $\mathbf{v} = -(3/2)\Omega x \mathbf{e}_y$. In addition, a weak vertical and azimuthal field permeates the plasma, so that $\mathbf{B} = B_y \mathbf{e}_y + B_z \mathbf{e}_z$.

We perturb this equilibrium with disturbances of the form $\propto e^{ik_x x + ik_z z + st}$, where k_x and k_z are real vertical wavenumber and s is a (complex) frequency. We omit the details of the resulting linearised equations, but present the fourth-order dispersion relation that ensues. For further details the reader may consult Kunz & Balbus (2004). The relation, though imposing, can be made more workable by adopting units so that $\Omega = 1$ and $v_{Az}^2 = B_z^2/(4\pi\rho) = 1$. We then obtain

$$s^4 + c_3 s^3 + c_2 s^2 + c_1 s + c_0 = 0. \quad (9)$$

The four coefficients are

$$\begin{aligned} c_3 &= k_z^2 (\delta^2 \varepsilon^{-2} + 1) \nu_i^{-1}, \\ c_2 &= \varepsilon^2 + 2k_z^2 + \delta^2 k_z^4 \varepsilon^{-2} \nu_i^{-2} + \frac{3}{2} \left(\frac{B_x}{B_z} \right) \left(\frac{k_x}{k_z} \right) k_z^2 \nu_i^{-1}, \\ c_1 &= c_3 (k_z^2 + \varepsilon^2), \\ c_0 &= k_z^2 (k_z^2 - 3\varepsilon^2) + \delta^2 k_z^4 \nu_i^{-2} \\ &\quad + \frac{3}{2} (k_z^2 + \varepsilon^2) \left(\frac{k_x}{k_z} \right) \left(\frac{B_y}{B_z} \right) k_z^2 \nu_i^{-1}, \end{aligned}$$

where

$$\varepsilon^2 = \left(1 + \frac{k_x^2}{k_z^2} \right)^{-1}, \quad \delta^2 = 1 + \frac{B_y^2}{B_z^2}.$$

We may consider s as a function of the vertical wavenumber k_z once the following parameters have been set: k_x/k_z , B_y/B_z , and ν_i .

3.3 Stability criterion

Marginal stability corresponds to $s = 0$, which permits us to obtain a stability criterion. In the simple case of channel modes, $k_x/k_z = 0$, instability occurs on all vertical wavenumbers satisfying

$$k_z^2 < \frac{3\nu_i^2}{\nu_i^2 + \delta^2}. \quad (10)$$

In the strongly coupled limit $\nu_i \gg 1$ we recover the classical ideal stability criterion for a Keplerian disc. But for smaller values of ν_i , instability only occurs on longer scales. Moreover, the presence of an azimuthal field ($\delta > 1$) further restricts the allowed range of wavenumbers and, as we shall see in the next section, the growth rates also suffer.

For non-zero k_x the stability criterion is a great deal more complicated (KB04). Instability occurs when

$$k_z^2 < 3\varepsilon^2 \frac{\nu_i^2 - \frac{1}{2}(k_x/k_z)(B_y/B_z)\nu_i}{\nu_i^2 + \delta^2 + \frac{3}{2}(k_x/k_z)(B_y/B_z)\nu_i}. \quad (11)$$

In the limit of $\nu_i \gg 1$, we recover the expected axisymmetric criterion in ideal MHD, $k_z^2 < 3\varepsilon^2$ (see for e.g. Latter et al. 2015). For moderate values of ν_i the range of permitted k_z is complicated and in fact, as pointed out by Kunz & Balbus (2004), the MRI can grow on a vastly extended range of k_z in a band of negative k_x/k_z (albeit with a much reduced growth rate). This phenomena highlights the role of ambipolar diffusion in mitigating the stabilising influence of magnetic tension on shorter scales. Field lines which would ordinarily prevent tethered fluid blobs from drifting apart via MRI can slip through them — and yet concurrently transport sufficient angular momentum for instability to proceed. Meanwhile, if the magnetic perturbations are appropriately oriented, then damping is minimised (see discussion in Desch 2004).

Finally, unstable modes must be able to fit into the disc. And thus $k_z > v_{Az}/c_s$, where c_s is the gas sound speed. Combined with criterion (11), this yields a maximum vertical field strength that instigates growth for a given mode.

3.4 Application to β Pic

In this section we adopt $\nu_i = 100$, and compute MRI growth rates versus wavenumber for various values of k_x/k_z and

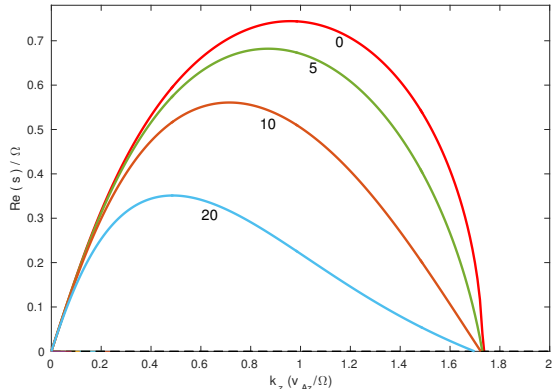


Figure 4. The real part of the MRI growth rate s as a function of vertical wavenumber k_z . Modes plotted are channel flows, with $k_x = 0$, and $\nu_i = 100$. The different curves correspond to $B_y/B_z = 0, 5, 10$, and 20 .

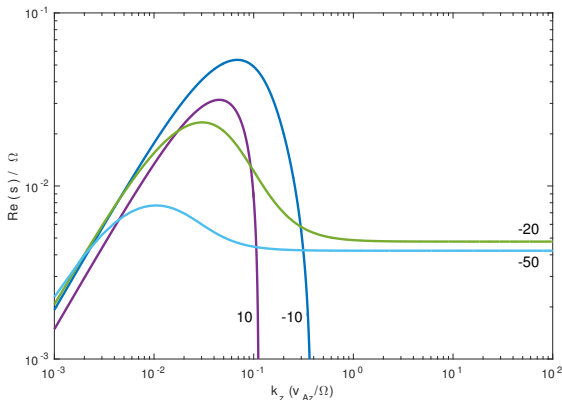


Figure 5. The real part of the MRI growth rate s as a function of vertical wavenumber k_z . Here $B_y/B_z = 5$, $\nu_i = 100$ and radial modes are plotted of different k_x . The four curves correspond to $k_x/k_z = -50, -20, -10$, and 10 .

B_y/B_z . We also discuss the stability criterion and give upper limits on the critical ambient magnetic field above which the MRI switches off.

In Figure 4 we plot the real part of the growth rate for channel modes, i.e. when $k_x = 0$. Four different background magnetic configurations are presented: $B_y/B_z = 0, 5, 10$, and 20 . Though the ions and neutrals are relatively well-coupled ($\nu_i = 100$), the growth rates deviate from the predictions of ideal MHD in that the stronger the azimuthal field, the weaker the growth: an effect clearly associated with ambipolar diffusion. The critical wavenumber of marginal stability, however, remains close to the classical value.

Modes exhibiting selected radial wavenumbers are presented in Figure 5 in the case of $B_y/B_z = 5$. We show growth rates when $k_x/k_z = -50, -20, -10$, and 10 . As pointed out in KB04, growth can persist on extremely small scales if the mode’s wavevector is oriented favourably, as in the cases of $k_x/k_z = -20$ and -50 . Such modes differ significantly from channel flows, as their wavevectors are almost perpendicular. Note, however, that their growth rates are over two orders of magnitude smaller.

The main question, when applying these results to β Pic, is whether unstable modes (exhibiting respectable growth rates) can actually fit into the vertical extent of the disc. Let us first consider the channel modes of Fig. 4. They require that $v_{Az} \lesssim c_s$, a criterion that can be reworked into a condition on the latent magnetic field

$$B_z \lesssim 4.1 \times 10^{-6} \left(\frac{T}{100 \text{ K}} \right)^{1/2} \left(\frac{n}{100 \text{ cm}^{-3}} \right)^{1/2} \text{ G}. \quad (12)$$

Using the estimates of Section 2, we find that at 10 AU, the vertical field must be less than about 10^{-4} G, while at 100 AU it must be less than $\sim 2 \times 10^{-6}$ G. It is clear that relatively weak fields stabilise the MRI, owing to the very low densities of the debris-disc gas. But unfortunately the magnetic environment of β Pic, or analogous debris discs, is difficult to constrain. As a guide, the Solar System’s interplanetary medium varies between 10^{-6} G and 10^{-5} (e.g. Jackman et al. 2005; Burlaga & Ness 2012). Of course, β Pic’s magnetic environment may differ markedly, it being forced by a young A-type star. Yet it is likely that at 100 AU channel modes are at best marginally stable to MRI channel modes, and quite possibly stable.

On the other hand, radial modes are far more difficult to stabilise, as illustrated in Figure 5. Their growth rates, however are $\lesssim 0.01\Omega$, yielding a linear growth time of $\gtrsim 10^5$ years. This is not only rather slow, but the ensuing turbulence may be insufficiently vigorous to supply the α values necessary to match the observations.

Finally note that this issue is complicated by the fact that once the MRI starts in one part of the disc, it can reconfigure the magnetic field at its current radial location and possibly at other locations as well, given sufficient time. Also the presence of an embedded planet’s magnetic field may also complicate the picture. The MRI will certainly be quenched in the vicinity of a planet with a strong internal dynamo, equivalent to Jupiter’s or Earth’s.

4 DISCUSSION

The previous section indicates that according to linear theory the MRI may arise at certain radii, but it is not guaranteed throughout the disc, at least in the form familiar from simulations of ideal MHD. The gas is too dilute, in particular at larger radii $\gtrsim 100$ AU. At these radii the more vigorous channel modes are possibly suppressed and activity proceeds via the slower growing radial modes. Whether we obtain the classical MRI or not comes down to the strength of the ambient magnetic field, which is poorly constrained.

However, let us suppose the latent field is sufficiently weak for the linear MRI to begin. What are the properties of its nonlinear saturated state? We are especially interested in how efficiently the ensuing turbulence can transport angular momentum. A number of numerical studies have been conducted probing MRI-induced turbulence with and without ambipolar diffusion. We now summarise these.

Simulations in purely local boxes have been performed by Hawley & Stone (1998) and Bai & Stone (2011). These show that when $\nu_i \sim 100$ the turbulence differs little from ideal MHD. Of note is that α increases as the plasma beta decreases; as we expect β to be low in the disc (because n is small), this hints that the accretion rate could be as high as

0.1, as required (Kral et al. 2016). Indeed, recent *ideal* MHD simulations using vertically stratified boxes show α as high as 1 when the plasma beta of the imposed vertical field dips below 100 (Salvesen et al. 2016). The disc, in these cases, becomes magnetically dominated, with its vertical structure controlled by magnetic pressure. It may be that debris disc gas, being so dilute, falls into this turbulent and magnetically dominated regime and thus exhibits the large alphas required by modelling and observations.

On the other hand, work incorporating both non-ideal MHD and vertically stratified boxes has focussed on the specific conditions of protoplanetary discs (Bai & Stone 2013a; Simon et al. 2013a,b). These simulations are strongly influenced by the vertical profiles of the ionisation fraction, which vary significantly from the surface to the midplane, where ν_i can dip to very low levels indeed. It is difficult to directly apply these results to the gas swathing debris discs, but they do sketch out possible behaviours that debris discs may exhibit. Of greatest interest is the suppression of the MRI and the launching of a magnetocentrifugal wind once the imposed vertical magnetic field grows too strong. Though mass is lost via the wind it also leads to significant angular momentum transport and hence radial accretion (e.g., Ogilvie 2012; Lesur et al. 2013). The effective α associated with this process may provide another route by which debris disc gas diffuses to smaller radii, as suggested by the modelling of observations (Section 2). In fact, given the expected lower betas at outer radii it is tempting to posit that the outer disc suffers a wind, while the inner radii undergo MRI turbulent accretion.

Obviously, many of these issues could be settled by dedicated vertically stratified simulations using vertical ionisation profiles appropriate for debris discs (as opposed to protoplanetary discs). Such computations could establish what kind of MHD behaviour develops at different radii in a model of β Pic, especially when the plasma beta is near (or less than) one. In this case, we may be able to determine whether radial MRI modes or disc winds induce sufficient transport to match the observations.

5 CONCLUSION

In this paper, we tested the linear stability of the gaseous envelope of a debris disc to the MRI. After giving a general theoretical framework to be applied to any debris disc, we focused on β Pic, which is the best characterised system. We showed that amongst the non ideal terms, the Ohmic dissipation and Hall effect can be neglected, while ambipolar diffusion is only moderately important in most parts of the disc. We show that given an ambient field less than a μG the MRI will grow in most parts of the gas disc ($\lesssim 200\text{AU}$). It is possible that even if stabilised by magnetic tension a magnetocentrifugal wind could be launched that would transport angular momentum in place of the MRI. The presence of a strong embedded magnetic field, such as around the planet β Pic b, would complicate the picture and may quench the MRI at the location of the planet. The model used in this paper could be used to assess the efficiency of MRI in other debris discs where the ionisation fraction, gas and electron densities might differ.

We propose some future work to be able to better quan-

tify the MRI or MHD processes (winds) at different radii through the disc. This could be done undertaking vertically stratified simulations of debris disc gas.

ACKNOWLEDGMENTS

We thank the referee for his/her valuable comments concerning the dust component. QK acknowledge support from the European Union through ERC grant number 279973. HNL is partially supported by STFC grant ST/L000636/1.

REFERENCES

- Bai, X.-N. 2011, *ApJ*, 739, 50
 Bai, X.-N., & Stone, J. M. 2011, *ApJ*, 736, 144
 Bai, X.-N., & Stone, J. M. 2013, *ApJ*, 767, 30
 Bai, X.-N., & Stone, J. M. 2013, *ApJ*, 769, 76
 Balbus, S. A., & Hawley, J. F. 1998, *Reviews of Modern Physics*, 70, 1
 Bell, K. R., Cassen, P. M., Klahr, H. H., & Henning, T. 1997, *ApJ*, 486, 372
 Blaes, O. M., & Balbus, S. A. 1994, *ApJ*, 421, 163
 Burlaga, L. F., & Ness, N. F. 2012, *ApJ*, 744, 51
 Carciofi, A. C., Bjorkman, J. E., Otero, S. A., et al. 2012, *ApJ*, 744, L15
 Cataldi, G., Brandeker, A., Olofsson, G., et al. 2014, *A & A*, 563, A66
 Czechowski, A., & Mann, I. 2007, *ApJ*, 660, 1541
 Dent, W. R. F., Wyatt, M. C., Roberge, A., et al. 2014, *Science*, 343, 1490
 Draine, B. T., & Sutin, B. 1987, *ApJ*, 320, 803
 Draine, B. T. 2011, *Physics of the Interstellar and Inter-galactic Medium* by Bruce T. Draine. Princeton University Press, 2011. ISBN: 978-0-691-12214-4
 Ferland, G. J., Porter, R. L., van Hoof, P. A. M., et al. 2013, *Revista Mexicana de Astronomia y Astrofisica*, 49, 137
 Fernández, R., Brandeker, A., & Wu, Y. 2006, *ApJ*, 643, 509
 Freudling, W., Lagrange, A.-M., Vidal-Madjar, A., Ferlet, R., & Forveille, T. 1995, *A & A*, 301, 231
 Goldreich, P., & Lynden-Bell, D. 1965, *MNRAS*, 130, 97
 Grigorieva, A., Thébault, P., Artymowicz, P., & Brandeker, A. 2007, *A & A*, 475, 755
 Guilet, J., Müller, E., Janka, H.-T., *MNRAS*, 447, 3992
 Hawley, J. F., & Stone, J. M. 1998, *ApJ*, 501, 758
 Hayashi, C. 1981, *Progress of Theoretical Physics Supplement*, 70, 35
 Heap, S. R., Lindler, D. J., Lanz, T. M., et al. 2000, *ApJ*, 539, 435
 Jackman, C. M., Achilleos, N., Bunce, E. J., et al. 2005, *Journal of Geophysical Research (Space Physics)*, 110, A10212
 King, A. R., Pringle, J. E., & Livio, M. 2007, *MNRAS*, 376, 1740
 Kral, Q., Thébault, P., & Charnoz, S. 2013, *A & A*, 558, A121
 Kral, Q., Wyatt, M., Carswell, R., Pringle, J., Matrà, L., & Juhász, A. 2016, *MNRAS*, *subm.*
 Kunz, M. W., & Balbus, S. A. 2004, *MNRAS*, 348, 355

- Latter, H. N., Fromang, S., & Faure, J. 2015, MNRAS, 453, 3257
- Lecavelier des Etangs, A., Vidal-Madjar, A., Roberge, A., et al. 2001, Nature, 412, 706
- Lesur, G., Ferreira, J., Ogilvie, G. I., 2013, A & A, 550, 61
- Lesur, G., Kunz, M. W., & Fromang, S. 2014, A & A, 566, A56
- Ogilvie, G. I., 2012, MNRAS, 423, 13180
- Olofsson, G., Liseau, R., & Brandeker, A. 2001, ApJ, 563, L77
- Roberge, A., Feldman, P. D., Weinberger, A. J., Deleuil, M., & Bouret, J.-C. 2006, Nature, 441, 724
- Roberge, A., Welsh, B. Y., Kamp, I., Weinberger, A. J., & Grady, C. A. 2014, ApJ, 796, L11
- Salvesen, G., Simon, J. B., Armitage, P. J., Begelman, M. C. 2016, MNRAS, 457, 857
- Sano, T., Inutsuka, S.-i., Turner, N. J., & Stone, J. M. 2004, ApJ, 605, 321
- Simon, J. B., Hawley, J. F., & Beckwith, K. 2009, ApJ, 690, 974
- Simon, J. B., Bai, X.-N., Stone, J. M., Armitage, P. J., & Beckwith, K. 2013, ApJ, 764, 66
- Simon, J. B., Bai, X.-N., Armitage, P. J., Stone, J. M., & Beckwith, K. 2013, ApJ, 775, 73
- Simon, J. B., Lesur, G., Kunz, M. W., & Armitage, P. J. 2015, MNRAS, 454, 1117
- Shakura, N. I., & Sunyaev, R. A. 1973, A & A, 24, 337
- Zagorovsky, K., Brandeker, A., & Wu, Y. 2010, ApJ, 720, 923